infrastructures

MDPI

Article

Research on the Cutting Efficiency of TBM Cutters in Jointed Rock Mass Based on a Multivariate Nonlinear Regression Model

Pengfei Song [1], Bingquan Liu [2], Zhiwen Tan [1], Chengzhi Yi [1], Jia Shi [1], Xin Xiang [2], Yue Peng [1], Junning Xie [3], Junfeng Liu [4], Hongzhi Cui [5] and Bolong Liu [5,*]

[1] China Construction Tunnel Construction Co., Ltd., Chongqing 401147, China
[2] China Construction International Construction Co., Ltd., Beijing 100029, China
[3] Beijing Daxing District Housing and Urban-Rural Development Commission, Beijing 102699, China
[4] School of Environment and Civil Engineering, Dongguan University of Technology, Dongguan 523808, China
[5] School of Civil Engineering, Shaoxing University, Shaoxing 312000, China; hongzhi.cui@usx.edu.cn
* Correspondence: 2021000164@usx.edu.cn

Abstract

The factors influencing the cutting efficiency of tunnel boring machine (TBM) cutters in jointed rock masses are very complex. To investigate TBM disc cutter cutting performance under variable cutter spacing and penetration depth, Particle Flow Code (PFC) 2D discrete element numerical simulation is carried out on a granite jointed rock mass. The numerical model adopts a disc cutter tip angle of 20° and tip width of 12 mm, joint spacing of 5 mm, joint inclination angle of 45°, and lateral confining pressure of 2.5 MPa; cutter spacing is set to 60, 80, 100, 120 mm, and penetration depth ranges from 2 mm to 10 mm as research variables. The force chain distribution, jointed rock mass failure modes, penetration load and cutting efficiency of disc cutters under different working conditions are systematically analyzed. An indicator for measuring the cutting efficiency called "crack propagation specific energy" is proposed. Based on the numerical simulation results, a complete quadratic multivariate nonlinear regression model is established to predict cutting efficiency. The results show that the optimal cutting performance occurs at a cutter spacing of 80 mm, where the shear failure proportion of contact bonds and cutting efficiency simultaneously reach the maximum, while incomplete penetration of joint failure surfaces and small cutting areas appear under 60 mm and 120 mm cutter spacing. With the increase in the disc cutter penetration depth, the shear failure proportion of contact bonds rises continuously, and the number of tensile failure microcracks gradually decreases. The research outcomes can provide a theoretical reference for TBM shield tunnel construction parameter optimization.

Keywords: rock breaking; efficiency; jointed rock mass; multivariate nonlinear regression

Academic Editor: Francesca Dezi

Received: 4 June 2026
Revised: 1 July 2026
Accepted: 8 July 2026
Published: 16 July 2026

1. Introduction

A tunnel boring machine (TBM) has become widely employed mechanized excavation equipment for long-distance, large-cross-section and deep-buried rock tunnels, with prominent advantages of high efficiency, safety, low environmental disturbance and strong geological adaptability [1,2]. In deep underground engineering, jointed rock masses are widely developed due to tectonic movement, geological loading and weathering. The discontinuity, anisotropy and heterogeneity caused by joints sharply change the stress propagation, crack evolution and fragmentation behavior of rock under TBM disc cutters, often inducing abnormal cutter wear, violent thrust–torque fluctuation, and low rock-breaking efficiency [3,4]. The rock-breaking mechanism of TBM disc cutters in jointed rock masses and high-precision prediction of the excavation efficiency are not only core scientific issues of cutter–rock interaction but also critical theoretical foundations for cutter layout optimization, operation parameter design and intelligent tunneling decision-making. Therefore, systematically studying the rock-breaking mechanism of TBM disc cutters in jointed rock masses and establishing a high-adaptability efficiency prediction model is of great theoretical value and engineering significance for improving tunneling efficiency, reducing construction costs and ensuring operation safety under complex geological conditions.

Over the past decades, researchers worldwide have conducted in-depth studies on the rock-breaking mechanism of TBM disc cutters under various geological conditions [5–7]. For intact hard rock, scholars have clarified that rock failure is dominated by tensile–shear crack propagation under high-concentrated contact stress. The indentation stress and rolling load jointly promote internal crack initiation, propagation and coalescence to form effective rock chips [8,9]. To improve the excavation performance, high-pressure water jet, microwave, laser and other auxiliary rock-breaking technologies have been developed, which can pre-damage rock, reduce the cutting force and prolong the cutter service life [10–12]. For jointed rock masses, joints become preferential paths for stress release and crack propagation, significantly changing the rock fragmentation mode and load response. Gong et al. (2005) and Feng et al. (2021) pointed out that joint orientation and spacing control the crack propagation direction and failure mode [13,14]. For soft rocks such as mudstone, the water-weakening effect is significant, which reduces the rock strength and brittleness, leading to plastic extrusion failure and high clogging risk [15,16]. For soft–hard composite strata, the excavation load fluctuates violently, and the overall efficiency is usually limited by hard rock intervals, resulting in uneven load distribution and accelerated cutter wear [17,18].

Extensive studies have also been carried out on TBM excavation efficiency evaluation, optimization and prediction [19–21]. In terms of rock-breaking performance evaluation, specific energy (SE) has been widely used as a core index, and the optimal cutter spacing–penetration ratio is recommended to maximize the excavation efficiency [22,23]. In terms of auxiliary rock-breaking reinforcement, Liu et al. (2026) confirmed that vibration assistance changes mineral particle movement from sliding to rolling, reducing cutter wear by 80–90% [1]. Xu et al. (2026) revealed that a high-pressure water jet with a cutting angle of approximately 60° obtains the lowest SE and the highest rock-breaking efficiency [2]. Lu et al. (2023) found that microwave irradiation linearly reduces the cutting force and exponentially decreases the specific energy with the increase in the irradiation time [24]. In terms of efficiency prediction, empirical models based on rock mass classification, uniaxial compressive strength (UCS) and joint indicators have been established [25,26]. With the development of big data and machine learning, data-driven models such as random forest (RF), long short-term memory (LSTM) and stacking ensemble learning have been applied to predict the penetration rate, thrust and torque, supporting intelligent parameter adjustment [27,28]. However, current models are mostly suitable for relatively intact or single lithology conditions, and few can realize stable and accurate efficiency prediction for jointed rock masses considering the coupling of joint characteristics, dynamic load and field construction factors.

In addition to joint development characteristics, lithological texture and homogeneity are core factors controlling the indentation feedback and brittle failure characteristics under disc cutter loading, and existing indoor indentation and numerical tests have revealed obvious differentiated rock-breaking responses among various rock types. For homogeneous intact rock, the rock matrix has uniform mineral distribution without internal weak planes. Under cutter indentation, high concentrated contact stress rapidly generates symmetric tensile radial cracks and shallow surface lateral cracks. High-brittleness homogeneous rock forms large complete rock chips at low penetration depth, and brittle spalling occurs instantly once the critical indentation load is reached, with an obvious sudden drop in the penetration force. Whereas low-brittleness homogeneous rock presents progressive plastic indentation, slow crack expansion and no obvious brittle collapse. For schistous foliated rock, continuous schistosity planes act as inherent weak interfaces, analogous to artificial jointed rock masses. During cutter indentation, cracks preferentially extend along foliation planes rather than penetrating the rock matrix. Strong brittle schist easily produces layered sheet fragments along schistosity under rolling indentation, and brittle splitting failure dominates the rock-breaking process; the indentation force fluctuates drastically due to the sequential splitting of thin rock sheets. For fine-grained rock, dense tiny mineral particles lead to high rock integrity and strong overall brittleness [29]. Under cutter indentation, microcracks initiate densely beneath the cutter tip and rapidly interconnect into penetrating fracture networks. The brittle failure threshold is low, and a small penetration depth can trigger a large-scale rock collapse, accompanied by the sharp attenuation of the indentation force. However, fine-grained rock lacks large-scale internal defects; so, the overall fragmentation uniformity is better without massive residual rock ridges. Compared with fine-grained rock, the indentation force curve shows more frequent small amplitude oscillations due to intermittent grain peeling and brittle grain boundary fracture. Overall, rock brittleness directly governs the critical indentation load, crack propagation velocity and fragment morphology for all four lithological categories. Brittle rock mass features rapid crack coalescence, low energy consumption for forming effective rock chips and obvious sudden force drop during indentation, while ductile rock presents slow energy-consuming plastic extrusion. Most existing studies separately discuss the indentation laws of single lithology, yet few systematically compare the coupling influence of brittle characteristics and structural planes on TBM cutting efficiency, which further motivates this numerical simulation research on brittle jointed granite [30,31].

In order to predict the cutting efficiency of TBM cutters, a numerical study was conducted on the cutting process of the jointed rock mass. An indicator for measuring the cutting efficiency called "crack propagation specific energy" was proposed. The existing SE index lacks the capacity to quantitatively characterize the correlation between microcrack failure modes (tensile failure and shear failure) and the overall tunneling efficiency. For jointed rock masses dominated by shear fracture, the conventional area-based specific energy cannot accurately correlate the proportion of shear microcracks with energy consumption, which restricts the analysis of the rock-breaking failure mechanism. To address the above drawbacks of traditional SE in jointed rock mass engineering evaluation, this study proposes a novel efficiency evaluation indicator named crack propagation specific energy, which takes the total propagation length of rock internal cracks as the statistical basis. It directly links the penetration load, penetration depth and crack expansion scale, effectively quantifies the energy consumed for crack growth along joints and rock matrix, and can accurately reflect the coupling influence of the joint characteristics and cutting parameters on the cutting efficiency. The breaking mechanism of the jointed rock mass under different cutter spacings and different penetration depths are also studied, and a sample library for predicting specific crack propagation is formed combining the obtained experimental data. Finally, a multivariate nonlinear regression model is proposed to predict the cutting efficiency, which can provide a reference for tunnel shield construction.

2. Establishment of the Numerical Model and Parameter Calibration

In the present study, a numerical model for the breaking of jointed rock mass under the disc cutters was established by PFC2D. In the model, the cutters are set as the wall unit; since the strength of the cutter is much more than the mechanical strength of the joint rock mass, the deformation of the cutter can be ignored. The specific parameters of the cutter are as follows: the tip angle is 20°, the tip width is 12 mm, and the cutter spacing is set as 80 mm. The joint spacing D is 50 mm, and the joint inclination angle α is 45°. The confining pressure at both sides of the specimen is 2.5 MPa. As shown in Figure 1, the rock is set as blue particles, and the joints are set as green particles. The rock mass model has a length of 200 mm and a width of 140 mm, with 46,399 particles. The penetration speed of the cutters is set through the built-in FISH language of PFC to simulate the penetration process of the cutters. In the model, the penetration load, penetration depth, and number of cracks are recorded. In order to observe the failure of the rock mass more intuitively under the action of the cutters, the FISH language is used to group and mark the particles causing joint failure in the model separately.

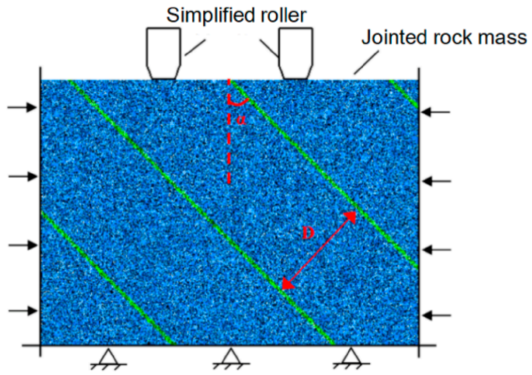

Figure 1. Particle flow model diagram of rock-breaking with cutter, where α is the joint inclination and D is the joint spacing.

In PFC 2D, the physical and mechanical properties of rocks are governed by both the contact conditions between individual particles and the intrinsic characteristics of the particles. Prior to establishing the numerical model, it is essential to determine micro-scale parameters based on the macroscopic mechanical behavior of the rock. These parameters include, but are not limited to, the maximum and minimum particle radii, porosity, particle friction coefficient, contact modulus, and parallel bond modulus, as well as the normal and tangential strengths of the parallel bonds. By simulating laboratory-scale material tests such as uniaxial compression tests and Brazilian tensile tests, the micro-scale parameters are calibrated until the numerical simulation results align with the experimental observations. This iterative process is referred to as PFC parameter calibration. Firstly, the whole PFC2D simulation is divided into four core command groups, executed sequentially via embedded FISH language. Model generation group: Create specimen boundary walls, generate rock matrix balls with radius range 0.3–0.5 mm, assign initial porosity 0.15, and implement servo-confining pressure command to maintain 2.5 MPa lateral constraint on side walls. Secondly, parallel bond contact models are assigned between rock balls and joint balls respectively; then, we input the calibrated micro-mechanical parameters (modulus, bond strength, friction coefficient) listed in Table 1. Thirdly, joint clusters are grouped, where green-colored balls form independent joint clusters to distinguish discontinuity planes from intact granite matrix and enable contact detection between rock clusters and joint clusters. Finally, two rigid cutter walls with fixed tip geometry are defined; then, we apply constant penetration velocity via FISH loop and record the real-time penetration force, crack number and bond failure information using hist monitoring commands.

Table 1. Mesoscopic parameters of jointed rock model materials.

Type	Particle Modulus (GPa)	Particle Stiffness Ratio	Parallel Modulus (GPa)	Parallel Bond Stiffness Ratio	Normal Bond Strength (MPa)	Normal Bond Strength (MPa)	Friction Coefficient
Granite	62	2.5	62	2.5	105	136	0.58
Joint	5.2	2.5	5.2	2.5	25	34	0.3

Based on the macroscopic mechanical properties of rock, including the density, uniaxial compressive strength, Poisson's ratio, and elastic modulus, both uniaxial compression tests and Brazilian splitting tests were performed using PFC2D to calibrate the microscopic parameters. In the uniaxial compression test, a cylindrical model with dimensions of 50 mm in diameter and 100 mm in height was employed, while in the Brazilian splitting test, a cylindrical model with a diameter of 50 mm was used, as illustrated in Figure 2. The particle radii within the models ranged from a minimum of 0.3 mm to a maximum of 0.5 mm, with an initial porosity set at 0.15. Particle interactions were governed by the parallel bond model, whereas the contact between the loading plates and the rock specimens was simulated using a linear contact model. By referencing the fundamental mechanical properties of granite and joints and through iterative calibration procedures, the final microscopic parameters for the jointed specimens were determined, as summarized in Table 1.

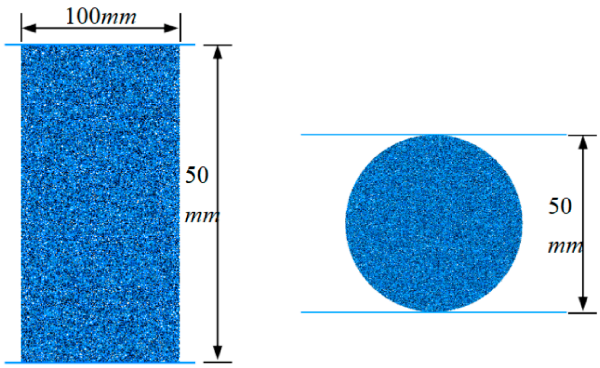

Figure 2. Numerical model of uniaxial compression test and Brazilian tensile tests.

3. Analysis of Cracking Behaviors of Joint Rock Mass and Cutting Efficiency of Disc Cutters

3.1. Cracking Behaviors of Joint Rock Mass and Cutting Efficiency of Cutters Under Different Cutter Spacings

To systematically reveal the coupling effect of adjacent disc cutters on the force chain transmission, joint crack penetration and cutting efficiency, the grouping design of cutter spacing follows the core philosophy of covering small spacing, optimal theoretical spacing and large spacing intervals to realize the comparative analysis of the cutter synergistic rock-breaking effect. Combined with the scaled model geometric similarity ratio and the widely recognized optimal cutter spacing range of hard rock TBM disc cutters in the existing research, four gradient values of 60 mm, 80 mm, 100 mm and 120 mm are set for comparative simulation [8,9]. Figure 3 shows the force chain and failure mode of rock under different cutter spacings. In this figure, the red regions indicate the fractured rock mass resulting from the action of the disc cutter, the green regions represent intact joints, and the blue regions correspond to unfractured rock. As observed in the figure, the presence of joint surfaces significantly influences the distribution of force chains within the rock mass. Particle contact forces are attenuated when transmitted across these discontinuities.

https://doi.org/10.3390/infrastructures11070241

Force chains exhibit a higher density between joint layers directly influenced by the cutter, with notable concentration beneath the cutter head. The existence of joint surfaces partially impedes the force chain transmission, while simultaneously promoting localized stress accumulation along the joints. This force chain configuration contributes to the formation of wing cracks at the joint surfaces and radial cracks beneath the cutter head. In models with cutter spacings of 80 mm and 100 mm, the two joint surfaces directly beneath the cutter heads are fully fractured, accompanied by denser force chain distributions. The force transmission preferentially follows the joint surfaces, leading to pronounced stress concentrations. Furthermore, in the 60 mm cutter spacing scenario, lateral cracks between adjacent cutters coalesce, generating elongated, thin rock fragments, while wing cracks initiate at the joint surfaces. An excessively dense cutter layout leads to severe over-crushing of the rock mass between adjacent cutters, generating a large number of slender flaky rock chips. First, these thin fragments are prone to being extruded and compacted in the cutterhead bucket and screw conveyor, easily causing mud caking and blockage of the mucking system, reducing the mucking efficiency and delaying tunneling progress. Second, thin rock fragments carry sharp edges, which will produce continuous abrasive scraping on the cutter sealing, cutterhead panel and conveying chute, accelerating the wear of metal components and increasing the frequency of cutter replacement and equipment maintenance costs. Third, over-crushing consumes extra rock-breaking energy, raising the overall specific energy of tunneling, resulting in higher thrust and torque fluctuation, increased energy consumption of the main driving system, and even triggering the overload alarm of the cutterhead. Conversely, for cutter spacing of 120 mm, the failure planes aligned with the joint surfaces do not fully propagate. Due to the large cutter spacing, the stress fields of neighboring disc cutters cannot overlap, and isolated independent rock breaking areas are formed without connected penetration cracks; thus, the joint planes between cutters cannot be fully fractured, and a large amount of intact rock ridges remain between adjacent cutting grooves, which cannot fall off automatically and need repeated secondary rolling extrusion by cutters. On the whole, the 60 mm spacing results in limited fracture zones, whereas the 120 mm spacing leads to isolated rock fragmentation patterns due to insufficient interaction between adjacent cutters.

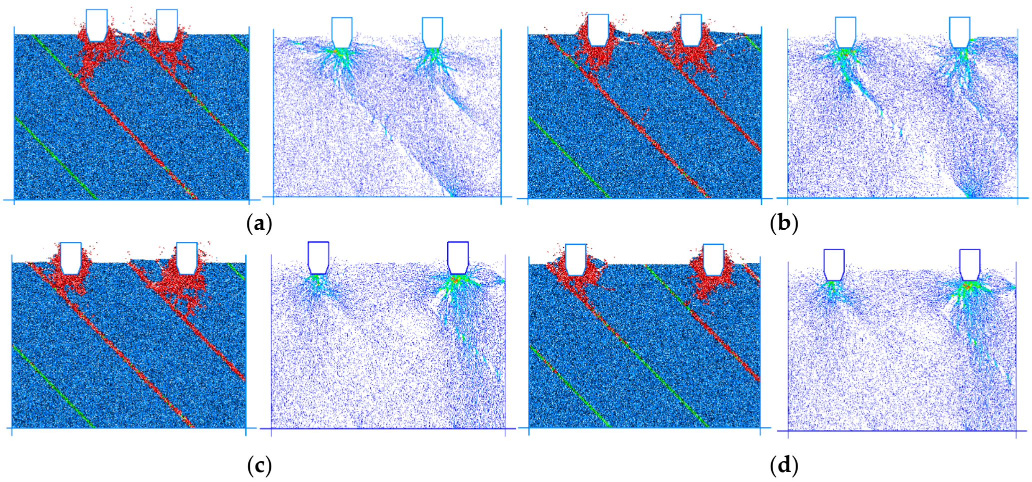

Figure 3. Force chain distribution diagram and failure modes of jointed rock mass under different cutter spacings, where the red regions indicate the fractured rock mass resulting from the action of the disc cutter, the green regions represent intact joints, and the blue regions correspond to unfractured rock: (**a**) cutter spacing of 60 mm; (**b**) cutter spacing of 80 mm; (**c**) cutter spacing of 100 mm; (**d**) cutter spacing of 120 mm.

In the discrete element model, particles are interconnected through contact bonds. Monitoring the fracture of these contact bonds provides insight into the propagation and failure mechanisms of rock fractures. This study quantitatively analyzed the number of contact bonds that failed in shear and tension during the cutting process, as illustrated in Figure 4. In the model with a cutter spacing of 80 mm, both the total number of contact bonds and the number of shear-failed bonds reached their peak values. In contrast, the model with a cutter spacing of 120 mm exhibited a significantly lower number of shear failures compared to other cases. Correspondingly, visual inspection of the rock failure patterns revealed that the 120 mm cutter spacing resulted in the least extensive damage, suggesting that rock fragmentation via shear failure is more effective.

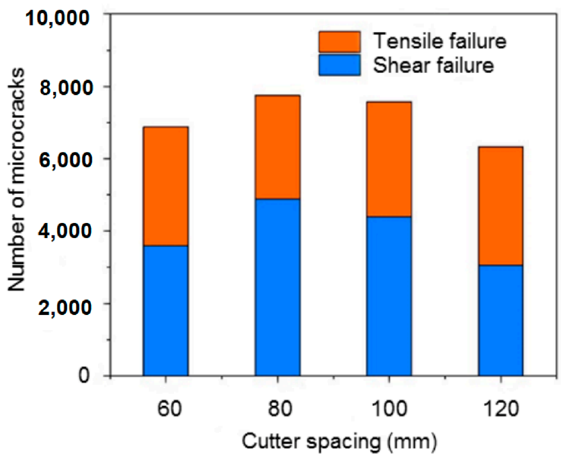

Figure 4. The number of microcracks under different cutter spacing.

Figure 5 shows the penetration force–penetration depth curves of rock mass under different cutter spacings. It can be seen that the trends of penetration force curves are similar with each other. The residual loads for the cutter spacing of 60 mm are more obvious, because the stress in the smaller broken area is more concentrated. In addition, the peak load for the cutter spacing of 100 mm is more than that for other spacings.

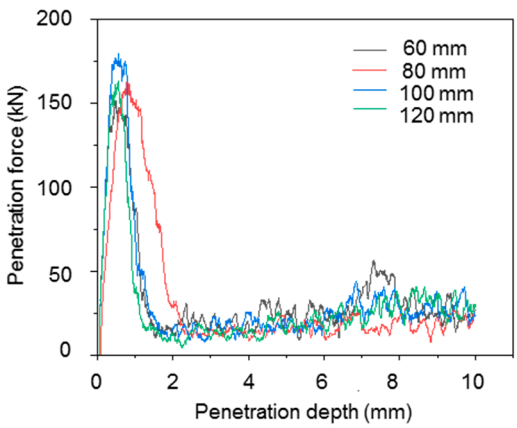

Figure 5. Penetration force–depth curve of cutter under different cutter spacings.

To reveal the cutting efficiency of cutters, the specific energy was calculated, which is defined as the energy consumed during the cutting process for a unit area of rock. In addition, the ratios of numbers of shear failure contact bonds to the total number of failed contact bonds under different cutter spacings were calculated, as illustrated in Figure 6. The black solid line represents the specific energy consumption per unit broken rock area, and the blue line denotes the proportion of shear-type contact bond failures. When the cutter spacing rises from 60 mm to 80 mm, the shear failure ratio increases sharply, while the specific energy declines to the minimum value, which proves that 80 mm spacing achieves optimal cutter rock-breaking efficiency with the lowest energy loss. For 100 mm and 120 mm cutter spacings, the shear failure proportion gradually drops, and the specific energy rises continuously, indicating a weakened synergistic cutting effect between adjacent cutters and deteriorated excavation performance. It can be observed that the variation trend of the specific energy with respect to the cutter spacing is precisely opposite to that of the shear crack ratio. When the cutter spacing is set to 80 mm, the specific energy required by the disc cutter reaches its minimum value, indicating the highest cutting efficiency, which coincides with the peak proportion of shear failure. This phenomenon can be attributed to the fact that excessively small cutter spacing leads to a highly concentrated breaking zone and excessive fragmentation of rock debris, thereby reducing the cutting efficiency. Conversely, when the cutter spacing is too large, each roller cutter operates independently, preventing the formation of effective crack propagation and interconnection, which also diminishes cutting efficiency. These findings suggest that when shear failure dominates the rock mass, the cutting efficiency of a disc cutter is enhanced.

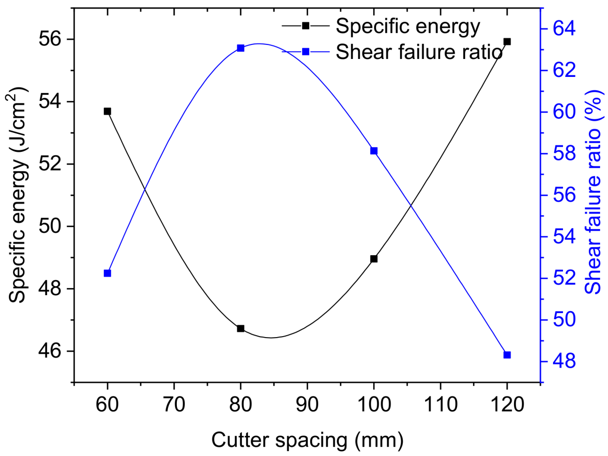

Figure 6. Specific energy and shear failure ratio under different cutter spacings.

3.2. Cracking Behaviors of Joint Rock Mass and Cutting Efficiency of Cutters Under Different Penetration Depths

The grouping design of penetration depth adheres to the philosophy of covering the whole process from initial shallow indentation to deep rolling cutting, to capture the evolution law of the rock failure mode from tensile-dominated to shear-dominated. Based on the penetration capacity of scaled disc cutters and the limit of the model specimen size, five gradient values of 2 mm, 4 mm, 6 mm, 8 mm and 10 mm with equal 2 mm intervals are selected. Figure 7 shows the force chain distribution and failure modes of rock mass under different penetration depths. According to the results, when the penetration depth reaches 2 mm, the joint surface beneath the right disc cutter is completely fractured, and the failure zone beneath the cutters extends to the joint surface. However, further crack propagation is impeded by the joint surface. In contrast, the force chain beneath the left disc cutter exhibits a higher concentration and broader force transmission, which results in relatively limited macroscopic rock failure beneath the left cutter compared to the right. When the penetration depth increases to 4 mm, additional damage occurs along the joint surface beneath the left disc cutter, with some cracks propagating toward the upper free surface, leading to the formation of minor rock debris. The force chain diagram indicates that although the right side still contains a larger concentrated force chain, the force chain density beneath the left cutter is higher, implying higher penetration force. As the disc cutter continues to penetrate deeper, the concentration of the force chain beneath the right cutter diminishes, and the force transmission and crack propagation predominantly occur beneath the left cutter. Simultaneously, lateral cracks beneath the disc cutter progressively develop and coalesce, resulting in the formation of discrete rock blocks on the free surface. Ultimately, when the penetration depth reaches 10 mm, the joint surface on the left remains incompletely fractured.

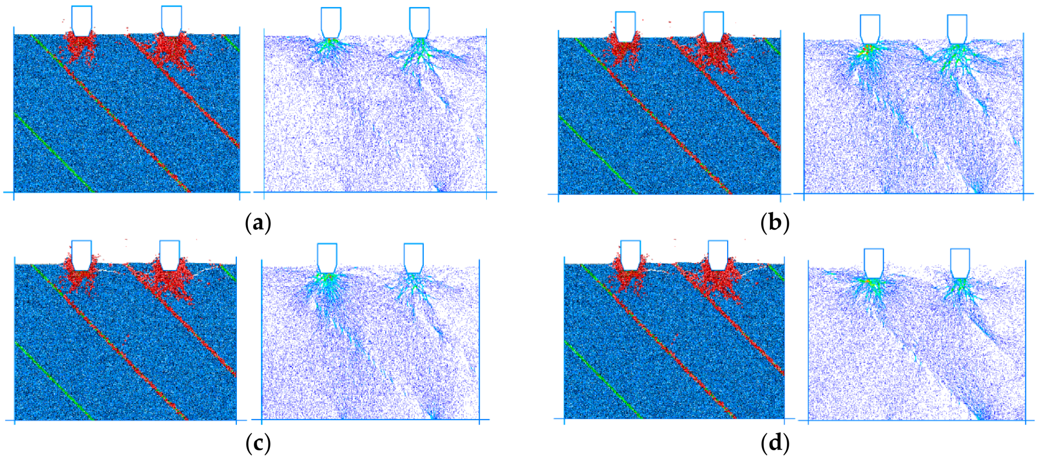

Figure 7. Force chain distribution diagram and failure diagram of rock mass under different penetration depths where the red regions indicate the fractured rock mass resulting from the action of the disc cutter, the green regions represent intact joints, and the blue regions correspond to unfractured rock: (**a**) penetration depth 2 mm; (**b**) penetration depth 4 mm; (**c**) penetration depth 6 mm; (**d**) penetration depth 10 mm.

Similarly, the total number of contact bond fractures and those caused specifically by shear failure under different penetration depths were obtained, as illustrated in Figures 8 and 9. In Figure 8, orange bars stand for tensile microcracks, and blue bars represent shear microcracks, which jointly reflect the evolution of the cutter rock-breaking performance as the penetration depth increases. With deeper cutter penetration from 2 mm to 10 mm, the total number of microcracks grows steadily, and the proportion of shear fractures rises persistently. Shear-dominated fragmentation generates uniform intact rock blocks and reduces redundant energy waste, thus continuously lifting the disc cutter excavation efficiency. At shallow penetration (2–4 mm), tensile cracking dominates and produces fragmented fine debris, resulting in higher energy consumption and poorer cutting performance.

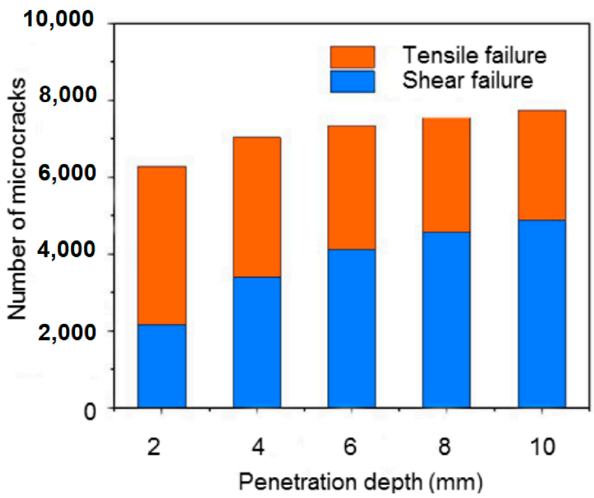

Figure 8. Number of microcracks under different penetration depths.

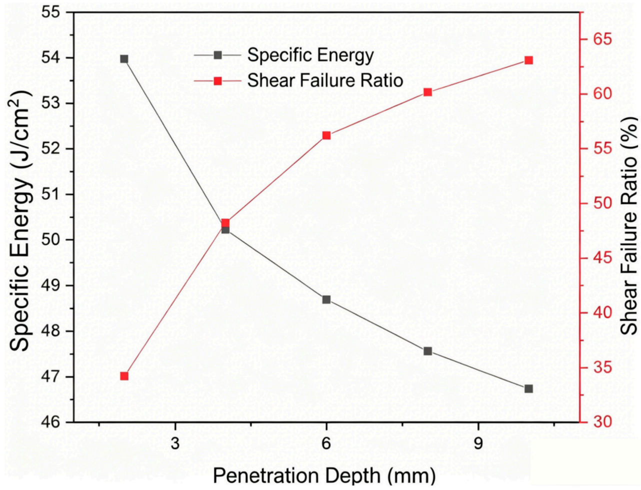

Figure 9. Specific energy and shear failure ratio under different penetration depths.

Figure 9 shows the comparison between the true simulated values and predicted values of crack propagation specific energy based on the multivariate nonlinear regression model, reflecting the model's capacity to predict cutter excavation efficiency under variable geological and mechanical parameters. Black solid dots denote the true crack propagation specific energy obtained from the PFC numerical tests, while red solid dots represent the model's predicted efficiency index. The two sets of data maintain consistent fluctuation trends and small deviation across all sample points, with a correlation coefficient R reaching 0.9353. This high fitting accuracy verifies that the proposed regression model can reliably forecast disc cutter rock-breaking efficiency under different cutter spacings, penetration depths and joint geometric conditions, providing quantitative efficiency prediction support for on-site TBM parameter adjustment. The results in Figures 8 and 9 indicate that both the total number of contact bond fractures and the number of shear-induced fractures increase with increasing penetration depth. Furthermore, by comparing the variation in specific energy with penetration depth, it can be observed that the trend of specific energy is inversely related to the proportion of shear fractures with respect to penetration depth. When the penetration depth reaches 10 mm, the cutting efficiency of the roller cutter is maximized. Additionally, it is evident that as the roller cutter continues to penetrate, the rate of increase in tensile fractures gradually decreases. This suggests that during the middle and later stages of rock failure, crack propagation is predominantly characterized by shear fractures, indicating that shear failure is the dominant failure mechanism. The above also explains the observed decrease in specific energy with increasing penetration depth.

4. Prediction of Cutting Efficiency Based with Multivariate Nonlinear Regression Model

According to the previous studies, the main factors influencing the cutting efficiency of disc cutters are the cutter spacing, penetration depth, joint spacing, and joint dip angle. In order to quantify the cutting efficiency of the disc cutters in the numerical model, an indicator called "crack propagation specific energy" is proposed. The term is defined as the energy consumed per unit length of crack propagation in the rock mass under rolling cutter static pressure, which can be calculated by $E_l = \frac{F_v p}{l}$, where E_l denotes the crack propagation specific energy, F_v is the vertical penetration force applied by disc cutter, p represents penetration depth of disc cutter into rock mass, and l is the total propagation length of surface cracks in jointed rock mass under corresponding penetration depth. In addition, a multivariate nonlinear regression model is proposed to predict the crack propagation specific energy. To enhance the understanding of the crack propagation specific energy, four independent variables—cutter spacing, penetration depth, joint spacing, and joint dip angle—are introduced. Multivariate nonlinear regression enables the quantification of the influence of each independent variable on the dependent variable.

The principle is as follows: multivariate nonlinear regression primarily involves constructing a mathematical model, estimating the unknown parameters within the model, assessing the model's reliability, and utilizing it for predictive analysis. Crack propagation specific energy is influenced by multiple factors. The developed multivariate regression model encompasses the following three primary mathematical formulations [32]:

① Pure quadratic model: $y = \beta + \sum \beta_i x_i + \sum \beta_{jj} x_j^2$

② Cross model: $y = \beta + \sum \beta_i x_i + \sum \beta_{jk} x_j x_k$

③ Complete quadratic model: $y = \beta + \sum \beta_i x_i + \sum \beta_{jk} x_j x_k$

Through the toolbox function in 1st Opt software and the general global optimization algorithm for computation, the most suitable multiple regression model for describing and explaining crack propagation behavior has been determined to be the complete quadratic model. The specific mathematical expression is as follows:

$$E_l = p_1 + p_2 DP + p_3 \alpha D + p_4 DS + p_5 \alpha P + p_6 PS + p_7 \alpha S + p_8 D + p_9 P + p_{10} \alpha + p_{11} D^2 + p_{12} P^2 + p_0$$

where D denotes the cutter spacing (in millimeters), P represents the penetration depth of the roller cutter (in millimeters), θ is the joint dip angle (in radians), and S stands for the joint spacing (in millimeters). The parameter values derived from the software calculations are listed in Table 2.

Table 2. Calculated values of parameters of multivariate nonlinear regression model.

Parameters	Calculated Value	Parameters	Calculated Value
p_0	0.9007	p_7	−0.005474
p_1	−0.001065	p_8	−0.01115
p_2	0.0003896	p_9	−0.6874
p_3	0.000017898	p_{10}	0.00007885
p_4	−0.002395	p_{11}	0.006409
p_5	−0.0001071	p_{12}	0.2824
p_6	0.0031		

A series of goodness-of-fit tests are conducted on the equations derived from the multivariate nonlinear regression model, which is shown in Table 3. The resulting performance metrics are then utilized to predict the specific energy consumption during crack propagation, which in turn allows for the evaluation of construction efficiency across various engineering scenarios. The primary goodness-of-fit measure employed in this study is the coefficient of determination (R^2). This statistic quantifies the proportion of the total variation in the dependent variable that is explained by the regression model, reflecting the extent to which changes in the independent variables account for variations in the dependent variable. Generally, a higher R^2 value indicates a higher proportion of variability in the dependent variable that can be attributed to the independent variables. The calculated values for each evaluation metric are summarized as follows:

Table 3. Multivariate nonlinear regression test index results.

Inspection Indicators	Calculated Value	Parameters	Calculated Value
Mean square deviation (RMSE)	0.03786	Square of the correlation coefficient (R^2)	0.8748
Sum of squared residuals (SSR)	0.1577	Adjusted R-squared (Adj. R^2)	−0.0341
Correlation coefficient (R)	0.9353	Determination coefficient (DC)	0.8748

It should be noted that $R^2 = 1 - \frac{(1-R^2)(n-1)}{n-k-1}$, where n is the total number of sample data groups, and k represents the number of independent regression variables. From statistical principles, the core reason for the negative adjusted R^2 in this study is that the complete quadratic multivariate nonlinear regression model adopted in this paper contains a large number of cross terms, quadratic terms and constant coefficients, resulting in a relatively high total number of independent variables k. In addition, the overall sample library established by PFC2D numerical simulation is limited, and the sample quantity n is not large enough relative to the model variable quantity. The basic determination coefficient $R^2 = 0.8748$ of the model is high, but after the penalty term $\frac{n-1}{n-k-1}$ for excessive variables is introduced, the penalty effect is amplified due to the insufficient sample size, which makes the calculated Adj.R^2 drop below zero. Statistically, a negative adjusted R^2 only means that the explanatory ability of the complete quadratic overfitting model is even weaker than the simple average model after deducting the penalty of redundant variables, which is a normal mathematical operation result and does not represent invalid model fitting.

The results of the model verification indicators demonstrate that the correlation coefficient R of the developed model is 0.9353, which indicates a strong goodness of fit. This model can be effectively utilized to predict the specific energy required for crack propagation. In the comparison between the model's predicted values and the experimentally obtained actual values, as presented in Figure 10, the overall trend of two curves maintains high consistency across all sample points without obvious systematic deviation, which reveals a generally consistent alignment. Consequently, this model can serve as a valuable reference for predicting tunneling efficiency under varying geological conditions and mechanical parameters. Figure 10 visually proves that the model can accurately quantify the energy consumption of crack expansion under diverse cutter layout and jointed rock mass conditions, and it can be adopted as an effective auxiliary tool to predict TBM rock-breaking efficiency in actual jointed granite tunnelling engineering.

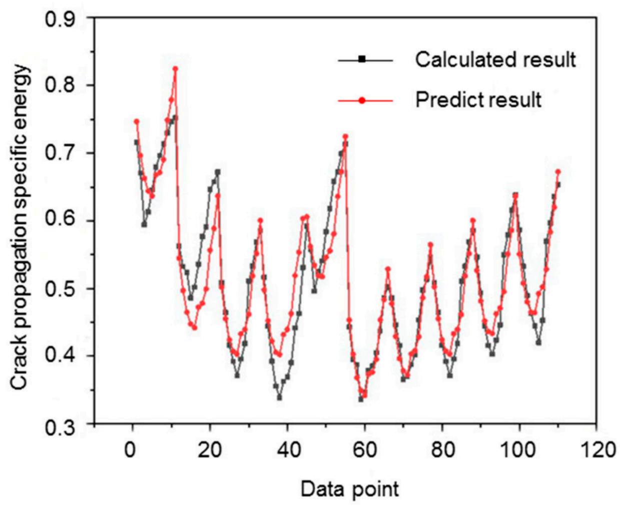

Figure 10. Comparison between the simulated true values and predicted values of the crack propagation specific energy based on the complete quadratic multivariate nonlinear regression model.

5. Conclusions

In this paper, PFC2D discrete element simulation is adopted to investigate the rock-breaking response of jointed granite under disc cutters, and the influences of cutter spacing and penetration depth on rock cracking characteristics and cutting efficiency are analyzed. In the present study, a multivariate nonlinear regression model for predicting the crack propagation specific energy is established based on simulation data. The novel crack propagation specific energy index and complete quadratic multivariate nonlinear regression model established in this paper are suitable for medium–high brittleness jointed crystalline hard rocks, primarily granite, granodiorite and similar igneous rock masses with regularly distributed persistent joints. The condensed core conclusions and on-site construction guidance suggestions are summarized as follows:

(1) Among the four tested cutter spacings, 80 mm is the optimal layout interval. Under this spacing, the joint surfaces are fully penetrated, and the shear failure proportion of contact bonds and cutting efficiency reach the maximum simultaneously. Too small (60 mm) or too large (120 mm) cutter spacing leads to incomplete joint penetration, narrow fracture zones and a poor synergistic rock-breaking effect between adjacent cutters.

(2) Increasing the penetration depth continuously elevates the shear failure ratio of rock contact bonds and reduces the tensile microcrack proportion. Shear fracture dominates rock mass damage in the late penetration stage, which reduces the crack propagation specific energy and significantly improves the overall rock-breaking efficiency.

(3) The proposed crack propagation specific energy indicator can quantitatively characterize the energy consumption of crack expansion in jointed rock masses. The established complete quadratic multivariate nonlinear regression model can accurately predict the cutting efficiency under variable cutter layout, penetration and joint geometric parameters.

It should be noted that variations in lateral confinement will remarkably change the force chain transmission, joint penetration degree and energy consumption of rock fragmentation. To fill this research gap, our follow-up research will comprehensively consider multi-level lateral confinement conditions at the excavation face. Combined with the optimal working conditions revealed by the simulation results for TBM construction in medium-buried jointed granite tunnels, it is suggested that when designing the disc cutter spacing of the TBM cutterhead for jointed granite with 45° dominant joints and 5 mm scaled joint spacing, one should take 80 mm as the reference optimal spacing and scale proportionally according to the actual model similarity ratio. Furthermore, under the premise of stable surrounding rock deformation, one should appropriately increase the single penetration depth of the disc cutters instead of shallow repeated rolling. Deep penetration promotes shear-dominated rock fragmentation, reduces energy consumption for rock breaking, lowers cutter wear rate and alleviates frequent thrust–torque fluctuation, which can effectively improve the daily tunneling advance rate in jointed rock tunnels.

Author Contributions: Conceptualization—P.S., methodology—Z.T., data collection and analysis—B.L. (Bingquan Liu), data curation and writing—J.X., B.L. (Bolong Liu) and J.L., original draft preparation—C.Y., J.S. and X.X., writing—review and editing and supervision—Y.P., Investigation —H.C. All authors have read and agreed to the published version of the manuscript.

Funding: This research was funded by the Joint Fund Program of Guangdong Basic and Applied Basic Research Foundation (Grant No. 2022A1515110766).

Data Availability Statement: No new data were created or analyzed in this study. The data used for analysis in this study were sourced from the literature cited as references. The original contributions presented in this study are included in the article. Further inquiries can be directed to the corresponding author.

Conflicts of Interest: Author Pengfei Song, Bingquan Liu, Zhiwen Tan, Chengzhi Yi, Jia Shi, Xin Xiang and Yue Peng was employed by the company China Construction Tunnel Construction Co., Ltd.and Beijing Daxing District Housing and Urban-Rural Development Commission. The remaining authors declare that the research was conducted in the absence of any commercial or financial relationships that could be construed as a potential conflict of interest.

References

1. Liu, B.L.; Lu, M.W.; Ruan, H.W.; Han, G.S.; Chen, H.; Gao, H.C.; Zhang, L.; Wang, S.; Guo, Y.B.; Ye, Y.Y.; et al. Experimental investigation on rock-breaking mechanism by scaled button cutters assisted by vibration with different amplitudes. *Rock Mech. Rock Eng.* **2026**, *59*, 1–18. [CrossRef]
2. Xu, C.; Zhu, Y.J.; Wang, Q.Y.; Liu, X.L.; Ren, G.F.; Wang, S.J. Influence of waterjet cutting angle on cutting efficiency by high-pressure waterjet-assisted TBM. *Rock Mech. Rock Eng.* **2026**, *59*, 1911–1930.
3. Xie, W.Q.; Zhang, X.P.; Hu, N. Real-time perception of rock-machine interaction information in TBM tunnelling using muck image analysis. *Tunn. Undergr. Space Technol.* **2023**, *136*, 105096. [CrossRef]
4. Ma, T.H.; Yu, S.H.; Liu, Y.M. Optimization of TBM tunnelling efficiency based on stacking ensemble learning. *Geomat. Nat. Hazards Risk* **2025**, *16*, 2555726. [CrossRef]
5. Xu, P.; Zou, J.; Huang, X.; Han, J. Numerical analyses of the influences of rock properties and joints on rock fragmentation in shaft sinking by drilling method. *Sci. Rep.* **2024**, *14*, 24870. [CrossRef] [PubMed]
6. Feng, P.; Cao, P.; Li, J.; Tang, R.; Li, H. Dynamic fracture mechanism and fragment characteristics of sandstone specimens with symmetrical conjugate fissures under static pre-compression. *Sci. Rep.* **2024**, *14*, 21268. [CrossRef] [PubMed]
7. Zhang, L.; Wang, E.Y.; Liu, Y.B.; Yue, W.T.; Chen, D. Experimental research into the dynamic damage characteristics and failure behavior of rock subjected to incremental repeated impact loads. *Eng. Geol.* **2024**, *331*, 107435. [CrossRef]
8. Cho, J.W.; Jeon, S.; Yu, S.H.; Chang, S.H. Optimum spacing of TBM disc cutters: A numerical simulation using the three-dimensional dynamic fracturing method. *Tunn. Undergr. Space Technol.* **2010**, *25*, 230–244. [CrossRef]
9. Moon, T.; Oh, J. A study of optimal rock-cutting conditions for hard rock TBM using the discrete element method. *Rock Mech. Rock Eng.* **2012**, *45*, 837–849. [CrossRef]
10. Cheng, J.; Yang, S.; Han, W.; Zhang, Z.; Jiang, Z.; Lu, J. Experimental and numerical study on the indentation behavior of TBM disc cutter on hard-rock precutting kerfs by high-pressure abrasive water jet. *Arch. Civ. Mech. Eng.* **2022**, *22*, 126. [CrossRef]
11. Ning, B.; Liu, F.; Liu, H.; Xia, Y. Experimental study on rock breaking using a microwave-assisted tunnel boring machine cutter. *Bull. Eng. Geol. Environ.* **2024**, *83*, 114. [CrossRef]
12. Rui, F.X.; Zhao, G.F. Experimental and numerical investigation of laser-induced rock damage and the implications for laser-assisted rock cutting. *Int. J. Rock Mech. Min.* **2021**, *139*, 104653. [CrossRef]
13. Gong, Q.M.; Zhao, J.; Jiao, Y.Y. Numerical modelling of the effects of joint orientation on rock fragmentation by TBM cutters. *Tunn. Undergr. Space Technol.* **2005**, *20*, 183–191. [CrossRef]
14. Feng, P.; Xu, Y.; Dai, F. Effects of dynamic strain rate on the energy dissipation and fragment characteristics of cross-fissured rocks. *Int. J. Rock Mech. Min.* **2021**, *138*, 104600. [CrossRef]
15. Wang, T.; Yin, C.Z.; Zheng, H.; Ke, W.H. Optimum spacing and rock breaking efficiency of TBM double disc cutters penetrating in water-soaked mudstone with FDEM. *Tunn. Undergr. Space Technol.* **2023**, *138*, 105174. [CrossRef]
16. Abu Bakar, M.Z.; Gertsch, L.S.; Rostami, J. Evaluation of fragments from disc cutting of dry and saturated sandstone. *Rock Mech. Rock Eng.* **2014**, *47*, 1891–1903.
17. Xie, Q.; Li, L.; Ma, Q.; Zhang, Z. Laboratory investigation of sandstone joints and strata on TBM performance using a tunnelling test platform. *Eng. Geol.* **2025**, *353*, 108133. [CrossRef]
18. Katuwal, T.B.; Panthi, K.K. TBM Penetration Rate Prediction in Himalayan Geology Using Machine Learning (ML) Techniques. *Rock Mech. Rock Eng.* **2026**, *59*, 4519–4551. [CrossRef]
19. Acaroglu, O.; Ozdemir, L.; Asbury, B. A fuzzy logic model to predict specific energy requirement for TBM performance prediction. *Tunn. Undergr. Space Technol.* **2008**, *23*, 600–608. [CrossRef]
20. Rostami, J. Performance prediction of hard rock tunnel boring machines (TBMs) in difficult ground. *Tunn. Undergr. Space Technol.* **2016**, *57*, 173–182. [CrossRef]
21. Hassanpour, J.; Rostami, J.; Tarigh Azali, S. Introduction of an empirical TBM cutter wear prediction model for pyroclastic and mafic igneous rocks. *Tunn. Undergr. Space Technol.* **2014**, *43*, 222–231. [CrossRef]
22. Samadi, H.; Mahmoodzadeh, A.; Hussein Mohammed, A.; Alenizi, F.A.; Ibrahim, H.H.; Nematollahi, M.; Elhag, A.B. Application of Several Fuzzy-Based Techniques for Estimating Tunnel Boring Machine Performance in Metamorphic Rocks. *Rock Mech. Rock Eng.* **2024**, *57*, 1471–1494. [CrossRef]
23. Zhang, K.; Liu, Q.; Zhang, Z. Simulation of Rock Breaking Based on FEM-CZM Method and Its Application in Disc Cutter Parameter Optimization. *KSCE J. Civ. Eng.* **2023**, *27*, 384–398. [CrossRef]
24. Lu, G.M.; Ding, C.; Zhou, J.J.; Liu, H.N.; Liu, C.Y. Influences of microwave irradiation on rock-breaking efficiency of a reduced-scale TBM cutter. *Appl. Sci.* **2023**, *13*, 4713.
25. Erharter, G.H.; Unterlass, P.; Radončić, N.; Marcher, T.; Rostami, J. Challenges and Opportunities of Data-Driven Advance Classification for Hard Rock TBM excavations. *Rock Mech. Rock Eng.* **2025**, *58*, 11387–11400. [CrossRef]
26. Karami, M.; Zare, S.; Rostami, J. Introducing an empirical model for prediction of disc cutter life for TBM application in jointed rocks: Case study, Kerman water conveyance tunnel. *Bull. Eng. Geol. Environ.* **2021**, *80*, 3853–3870. [CrossRef]

https://doi.org/10.3390/infrastructures11070241

27. Guo, D.; Li, J.H.; Jiang, S.H.; Xu, L.; Chen, Z.Y. Intelligent assistant driving method for tunnel boring machine based on big data. *Acta Geotech.* **2022**, *17*, 1019–1030.
28. Katuwal, T.B.; Panthi, K.K.; Basnet, C.B. Machine Learning Approach for Rock Mass Classification with Imbalanced Database of TBM Tunnelling in Himalayan Geology. *Rock Mech. Rock Eng.* **2025**, *58*, 11293–11318.
29. Jeong, H.Y.; Jeon, S. Characteristic of size distribution rock chip produced by rock cutting with a pick cutter. *Geomech. Eng.* **2018**, *15*, 811–822. [CrossRef]
30. Innaurato, N.; Oggeri, C.; Oreste, P. Laboratory tests to study the influence of rock stress confinement on the performances of TBM discs in tunnels. *Int. J. Miner. Metall. Mater.* **2011**, *18*, 253–259. [CrossRef]
31. Zhang, R.Q.; Su, D. Study on the influence of revolving patterns of cutterheads on tunneling operations concerning the box-jacking construction with an extra large rectangular tunnel profile via discrete-continuum coupling. *Comput. Geotech.* **2024**, *176*, 106735. [CrossRef]
32. Ling, J.X.; Yang, X.J.; Wu, Z.H. A Prediction method for TBM cutterhead dynamic tunneling performance under typical composite geological conditions. *Mech. Eng. Sci.* **2019**, *1*, 33–41. [CrossRef]

https://doi.org/10.3390/infrastructures11070241